Journal of Engineering Mathematics **30:** 487–499, 1996.

Open channel flow past a bottom obstruction

YINGLONG ZHANG and SONGPING ZHU
Department of Mathematics, The University of Wollongong, Wollongong, NSW 2522, Australia

Received 29 June 1994; accepted in revised form 30 August 1995

Abstract. A new nonlinear integral-equation model is derived in terms of hodograph variables for free-surface flow past an arbitrary bottom obstruction. A numerical method, carefully chosen to solve the resulting nonlinear algebraic equations and a simple, yet effective radiation condition have led to some very encouraging results. In this paper, results are presented for a semi-circular obstruction and are compared with those of Forbes and Schwartz [1]. It is shown that the wave resistance calculated from our nonlinear model exhibits a good agreement with that predicted by the linear model for a large range of Froude numbers for a small disturbance. The small-Froude-number non-uniformity associated with the linear model is also discussed.

Key words: Free-surface flows, nonlinear integral equations, channel flow, bottom topography, hodograph method.

1. Introduction

Free-surface flow past an obstruction sitting on the bottom or an object submerged in the fluid is a classical problem studied thoroughly using linearized models. A good summary can be found in Lamb [2] and Wehausen and Laitone [3]. However, only recently have researchers begun to study the nonlinear version of the problem (e.g., [4–10, 18]). Of particular interest and importance (e.g., in ship research) is the situation where nonlinear waves are generated downstream. For this type of problem, so far, emphasis has been placed on the case of infinite fluid depth. For the case of finite fluid depth (open channel flow problems), Forbes and Schwartz [1] proposed an integro-differential equation model using conformal mappings for the case of a semi-circular or semi-elliptic obstruction. However, their method was restricted by the conformal mappings that are necessary in their method to formulate the integro-differential equation. This deficiency was later remedied by King and Bloor [18] with a generalized Schwarz-Christoffel transformation.

In this paper, a fully nonlinear model based on integral equations is derived via hodograph transforms. Our model can be applied to an arbitrary shape of obstruction. However, the numerical approach used to solve the integral equations must be carefully chosen in order to overcome the difficulty that one of the equations is not well-conditioned. In view of this, a scheme proposed by Niessner [11] is adopted. Numerical results are calculated for the case of a semi-circular obstruction and are compared with the linearized results [1] and those of Forbes and Schwartz [1]. A reasonable agreement between the two nonlinear models is generally observed. Furthermore, it is shown that the wave resistance calculated from our model matches with that predicted by the linear model for moderate and large Froude numbers for a *small* disturbance. For small Froude numbers, it is shown that the linearized results give rise to large errors due to the small-Froude-number non-uniformity previously discussed by Dagan [5] and Doctors and Dagan [12] *et al.* for similar problems.

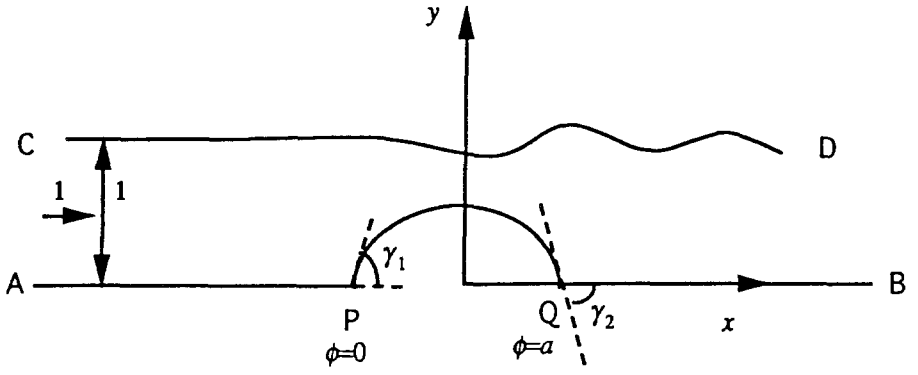

Fig. 1. A definition sketch.

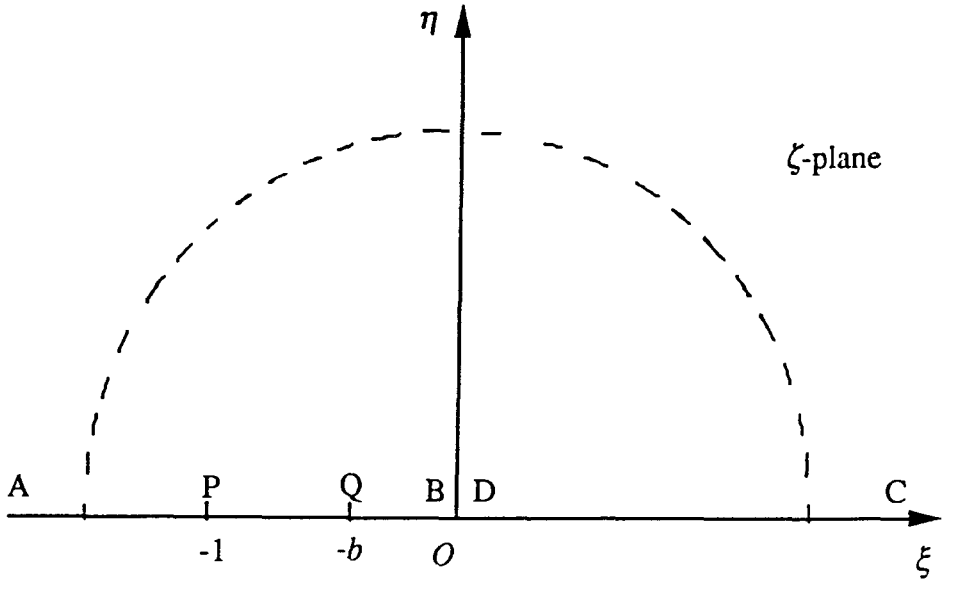

Fig. 2. The ζ-plane.

2. Mathematical formulation of the problem

Consider a two-dimensional potential flow of an inviscid and incompressible fluid past an obstruction sitting on the bottom (Figure 1). In this paper, we shall only discuss the case where uniform waves are generated far downstream, while far upstream the flow is assumed to be uniform with velocity c and of depth h_0. The effect of gravity is taken into consideration. All variables are made dimensionless with respect to h_0 or c or their combinations. It can be easily shown that the problem is defined via the Froude number $F = c/\sqrt{gh_0}$ and some other dimensionless geometrical parameters depending on the shape of the obstruction. After nondimensionalization, the fluid depth far upstream and the velocity there are equal to 1.

Due to the irrotationality and incompressibility, there exist a potential function and ϕ and a stream function ψ, and therefore a complex potential $f = \phi + i\psi$, which is an analytical function of $z = x + iy$. Since the total discharge is equal to 1, we can set the bottom and the

free surface to be the streamlines with $\psi = -1$ and $\psi = 0$ respectively. With a conformal mapping

$$\zeta = e^{-\pi f}, \tag{1}$$

the region occupied by the fluid is mapped into the upper half of the the ζ-plane and the bottom and the free surface respectively, are mapped onto the negative and positive real axes (Figure 2). Notice that the region far upstream has been mapped onto infinity, which, upon using Cauchy's integral formula, will result in an integral equation defined on the real axis only.

Introducing hodograph (logarithmic velocity) variables $\Omega \equiv \delta + \mathrm{i}\tau$ via

$$u - \mathrm{i}v \equiv f'(z(\zeta)) = e^{-\mathrm{i}\Omega(\zeta)}, \tag{2}$$

we can easily verify that δ represents the direction of the velocity ($-\pi \leqslant \delta < \pi$) and e^{τ} is the magnitude of the velocity. Since the flow is uniform far upstream, $\Omega \to 0$ as $|\zeta| \to \infty$. Utilizing Cauchy's integral formula in the upper half of the ζ-plane, we obtain

$$\Omega(\zeta) = \frac{1}{2\pi \mathrm{i}} \fint_{-\infty}^{\infty} \frac{\Omega(\zeta_0)}{\zeta_0 - \zeta} \mathrm{d}\zeta_0, \quad \text{for} \quad \mathrm{Im}\zeta > 0, \tag{3}$$

where $\fint$ stands for the Cauchy principal value of the integration. As ζ approaches the real axis from above, equation (3) becomes

$$\Omega(\zeta) = \frac{1}{\pi \mathrm{i}} \fint_{-\infty}^{\infty} \frac{\Omega(\zeta_0)}{\zeta_0 - \zeta} \mathrm{d}\zeta_0, \quad \text{for} \quad \mathrm{Im}\zeta = 0, \tag{4}$$

or

$$\tau(\zeta) = -\frac{1}{\pi} \fint_{-\infty}^{\infty} \frac{\delta(\zeta_0)}{\zeta_0 - \zeta} \mathrm{d}\zeta_0, \tag{5}$$

$$\delta(\zeta) = \frac{1}{\pi} \fint_{-\infty}^{\infty} \frac{\tau(\zeta_0)}{\zeta_0 - \zeta} \mathrm{d}\zeta_0, \tag{6}$$

after a separation into real and imaginary parts. By definition, $\delta(\zeta_0) = 0$ for $-\infty < \zeta_0 \leqslant -1$ or $-b \leqslant \zeta_0 \leqslant 0$, and therefore

$$\tau(\zeta) = -\frac{1}{\pi} \left(\fint_{-1}^{-b} + \fint_{0}^{\infty} \right) \frac{\delta(\zeta_0)}{\zeta_0 - \zeta} \mathrm{d}\zeta_0, \quad \text{for} \quad -1 \leqslant \zeta \leqslant -b \text{ or } \zeta > 0. \tag{7}$$

Before we go on to the next equation, it is advantageous to examine some possible singularities when stagnation points are present on the bottom. A stagnation point in the flow field results from the discontinuity of the derivative of the bottom contour line. Obviously, at a stagnation point, τ is infinite. The singularity depends on the contact angles γ_1 and γ_2 (cf. Figure 1) between the obstruction and the horizontal part of the bottom. If $\gamma_1 = \gamma_2 = 0$, i.e., for a smooth contact, there is no stagnation point and therefore τ is defined everywhere on the bottom. If, however, $0 < \gamma_1 < \pi$ or $-\pi < \gamma_2 < 0$, there is at least one stagnation point where τ is undefined. Let us take, for instance, $0 < \gamma_1 < \pi$. In this case, we have from equation (7)

$$\tau(\zeta) \sim -\frac{1}{\pi} \fint_{-1}^{-b} \frac{\delta(\zeta_0) - \delta(\zeta)}{\zeta_0 - \zeta} \mathrm{d}\zeta_0 - \frac{1}{\pi} \fint_{-1}^{-b} \frac{\delta(\zeta)}{\zeta_0 - \zeta} \mathrm{d}\zeta_0, \quad \text{as} \quad \zeta \to -1, \tag{8}$$

in which the first integral is non-singular, and hence

$$\tau(\zeta) \sim -\frac{\delta(-1)}{\pi} \log\left(\frac{-b-\zeta}{1+\zeta}\right), \tag{9}$$

which shows that $e^{-\tau}$ (i.e., the inverse of the magnitude of velocity) is only weakly singular at $\zeta = -1$ because $0 < \delta(-1)/\pi = \gamma_1/\pi < 1$.

On the other hand, for the case $-\pi < \gamma_1 < 0$ and $0 < \gamma_2 < \pi$, i.e., when a 'pit' instead of an obstruction is present on the bottom, the velocity at the contact points is infinite and therefore $e^{-\tau} = 0$ at these points. In conclusion, $e^{-\tau}$ is either finite or weakly singular on the bottom. These result can also be understood from the viewpoint of flow past a corner or wedge.

Bearing these results in mind, we can then derive (x, y) in terms of the independent variable ζ and dependent variables τ and δ. From equation (2) we have

$$\frac{\mathrm{d}z}{\mathrm{d}f} = e^{\mathrm{i}\Omega}. \tag{10}$$

But as $\mathrm{d}z/\mathrm{d}f = \mathrm{d}z/\mathrm{d}\zeta \cdot \mathrm{d}\zeta/\mathrm{d}f = -\pi\zeta \mathrm{d}z/\mathrm{d}\zeta$, two ordinary differential equations are obtained on the real axis of the ζ-plane

$$\frac{\mathrm{d}x}{\mathrm{d}\zeta} = -\frac{e^{-\tau}}{\pi\zeta}\cos\delta, \tag{11}$$

$$\frac{\mathrm{d}y}{\mathrm{d}\zeta} = -\frac{e^{-\tau}}{\pi\zeta}\sin\delta, \tag{12}$$

the integration of which yields (x, y) in terms of ζ, τ and δ. Since $e^{-\tau}$ is at worst weakly singular at some points on the bottom, x and y are well-defined everywhere.

Now the second equation linking the unknowns τ and δ can be obtained from the Bernoulli equation on the free surface. The nondimensionalized Bernoulli equation is

$$y + \frac{F^2}{2}(u^2 + v^2) = \frac{F^2}{2} + 1. \tag{13}$$

By definition, $u^2 + v^2 = e^{2\tau}$. Integrating (12) along the free surface, we have

$$y = 1 + \frac{1}{\pi}\int_{\zeta}^{\infty} \frac{e^{-\tau(\zeta_0)}}{\zeta_0}\sin\delta(\zeta_0)\,\mathrm{d}\zeta_0. \tag{14}$$

Substituting these relations in (13), differentiating both sides of (13) with respect to ζ, and then rearranging and integrating it with respect to ζ we are led to

$$\tau(\zeta) = \frac{1}{3}\log\left[1 - \frac{3}{\pi F^2}\int_{\zeta}^{\infty}\frac{\sin\delta(\zeta_0)}{\zeta_0}\,\mathrm{d}\zeta_0\right], \quad \text{for} \quad \zeta > 0, \tag{15}$$

which can be combined with (7) for $\zeta > 0$ to give

$$0 = \frac{1}{3}\log\left[1 - \frac{3}{\pi F^2}\int_{\zeta}^{\infty}\frac{\sin\delta(\zeta_0)}{\zeta_0}\,\mathrm{d}\zeta_0\right] + \frac{1}{\pi}\left(\int_{-1}^{-b} + \int_{0}^{\infty}\right)\frac{\delta(\zeta_0)}{\zeta_0 - \zeta}\,\mathrm{d}\zeta_0, \quad \text{for} \quad \zeta > 0. \tag{16}$$

Equations (7) and (16) are incomplete, unless some geometrical conditions on the obstruction and the boundary condition far upstream (radiation condition) are supplemented. For a semi-circular obstruction, we can define a dimensionless parameter $\alpha = r/h_0$, with r being the radius of the obstruction and it is easy to show there exists a two-parameter (α, F) family of solutions. Furthermore, in this case, we have a geometrical relation on the obstruction

$$x\cos\delta + y\sin\delta = 0, \quad \text{for} \quad -1 \leqslant \zeta \leqslant -b. \tag{17}$$

Integrating (11) and (12) along the obstruction gives

$$x(\zeta) = -\alpha - \frac{1}{\pi} \int_{-1}^{\zeta} \frac{e^{-\tau(\zeta_0)}}{\zeta_0} \cos\delta(\zeta_0)\, \mathrm{d}\zeta_0, \tag{18}$$

$$y(\zeta) = -\frac{1}{\pi} \int_{-1}^{\zeta} \frac{e^{-\tau(\zeta_0)}}{\zeta_0} \sin\delta(\zeta_0)\, \mathrm{d}\zeta_0. \tag{19}$$

A geometrical equation is thus obtained by substituting (18) and (19) into (17) as

$$0 = \alpha\pi\cos\delta(\zeta) + \int_{-1}^{\zeta} \frac{e^{-\tau(\zeta_0)}}{\zeta_0} \cos[\delta(\zeta_0) - \delta(\zeta)]\, \mathrm{d}\zeta_0, \quad \text{for} \quad -1 \leqslant \zeta \leqslant -b. \tag{20}$$

In view of the singularity in $e^{-\tau}$ (cf. (9)), we introduce a new variable t by

$$t(\zeta) = e^{-\tau(\zeta)}\sqrt{(1+\zeta)(-b-\zeta)}, \tag{21}$$

with which equation (20) becomes

$$0 = \alpha\pi\cos\delta(\zeta) + \int_{-1}^{\zeta} \frac{t(\zeta_0)}{\sqrt{(1+\zeta_0)(-b-\zeta_0)}} \cdot \frac{\cos[\delta(\zeta_0) - \delta(\zeta)]}{\zeta_0}\, \mathrm{d}\zeta_0,$$
$$\text{for} \quad -1 \leqslant \zeta \leqslant -b. \tag{22}$$

Notice that the singularities in (22) have been isolated to the denominator to facilitate a numerical computation.

With regard to the radiation condition at infinity (far upstream), Forbes and Schwartz [1] and Scullen and Tuck [13] proposed that the 'correct' condition be defined as the one that removes upstream 'spurious' waves in a numerical calculation. Probably due to the presence of derivative terms in their integro-differential equation model, Forbes and Schwartz [1] did not succeed in completely eliminating those upstream waves. Scullen and Tuck [13] proposed, in their work on flow past an object submerged in a fluid of infinite depth, a rather involved condition which successfully eliminated the upstream waves. The radiation condition we used is rather simple and effective, which will be shown in the next section.

3. Numerical method

If one discretizes the free surface and the obstruction equally along the real axis of the ζ-plane, nodal points tend to crowd towards upstream and poor results will be generated. On the other hand, an equal discretization in the potential function ϕ would yield an almost equal discretization in space (because far upstream $\phi \to x$ and if the wave amplitudes are small, far downstream $\phi \approx x$ as well; only in a small region near $x = 0$ the nodal spacing is distorted).

Therefore a change of independent variable from ζ to ϕ was made in equations (7), (16) and (22).

First of all, the free surface was truncated at two points $\phi_1^{(1)}$ and $\phi_{N+1}^{(1)}$ which represent far downstream and upstream, respectively. The truncated free surface was then discretized into N segments $[\phi_i^{(1)}, \phi_{i+1}^{(1)}]$ $(i = 1, 2, \ldots, N)$ of equal length. Similarly the semi-circular obstruction $[0, a]$ was also discretized into M small segments $[\phi_j^{(2)}, \phi_{j+1}^{(2)}]$ $(j = 1, 2, \ldots, M)$ with $\phi_1^{(2)} = 0$ and $\phi_{M+1}^{(2)} = a$. The integral equations were then discretized and solved with a collocation method. The singularity in equation (16) was subtracted from the Cauchy principal value integral, resulting in a non-singular integral plus a logarithmic term. The integration in each segment was carried out either analytically or by means of the ordinary Simpson rule. The resulting nonlinear algebraic equations were solved with an IMSL subroutine DNEQNJ, which employs a variation of Newton's method. The linearized solution derived by Forbes and Schwartz [1] was generally used as an initial guess, but when α was too large, the previously computed nonlinear solution for a smaller α was used instead. The numerical efficiency is reflected by the fact that it generally took only 3 CPU minutes on a SUN 4/470 Sparc Server to obtain a nonlinear solution when 181 points were placed on the free surface and 81 points were placed on the obstruction.

However, care must be taken with the interpolation and collocation schemes adopted in the discretization. The nonlinear equations are well-conditioned, except equation (16), which is essentially a Fredholm integral equation of the first kind with a singular kernel of Cauchy type. For this kind of integral equation, Niessner [11] showed that the condition number can be as good as that of a Fredholm integral equation of the second kind, provided that proper interpolation and collocation schemes are employed. He also gave a heuristic argument for the proper choice of interpolation and collocation schemes. As an example, in our case, if piecewise constant interpolation functions are used to approximate the unknowns on the free surface with collocation points being located in the middle of each segment, the Cauchy-type singularity (which is an 'anti-symmetric' singularity) tends to cancel out, resulting in a Jacobian with non-dominant diagonal entries and therefore a very poor conditioning of the nonlinear algebraic system. Following Niessner's [11] suggestion, we adopted a scheme with piecewise linear interpolation functions to approximate the unknowns on the free surface and the collocation points being placed at N mid-points $\phi_{i-1/2}^{(1)}$ $(1 = 1, 2, \ldots, N)$. On the obstruction one can use linear interpolation as well, but this is not necessary. To maximize numerical efficiency, we adopted piecewise constant interpolation functions to approximate the unknowns on the obstruction.

Lastly, but not least importantly, a radiation condition is needed to close the system. We found that by demanding the direction of the flow velocity at the last two upstream points to be equal to each other, i.e.,

$$\delta_{N-1} = \delta_N, \tag{23}$$

the upstream waves were entirely eliminated. According to Forbes and Schwartz [1] and others, equation (23) is the proper radiation condition. Such a radiation condition is not only intuitive but also simple to be implemented numerically; it amounts to placing a rigid horizontal wall far upstream.

After the unknown t, δ and a are found, the free-surface profile can be obtained by an integration of (11) and (12) along the free surface. However, there is a difficulty in finding

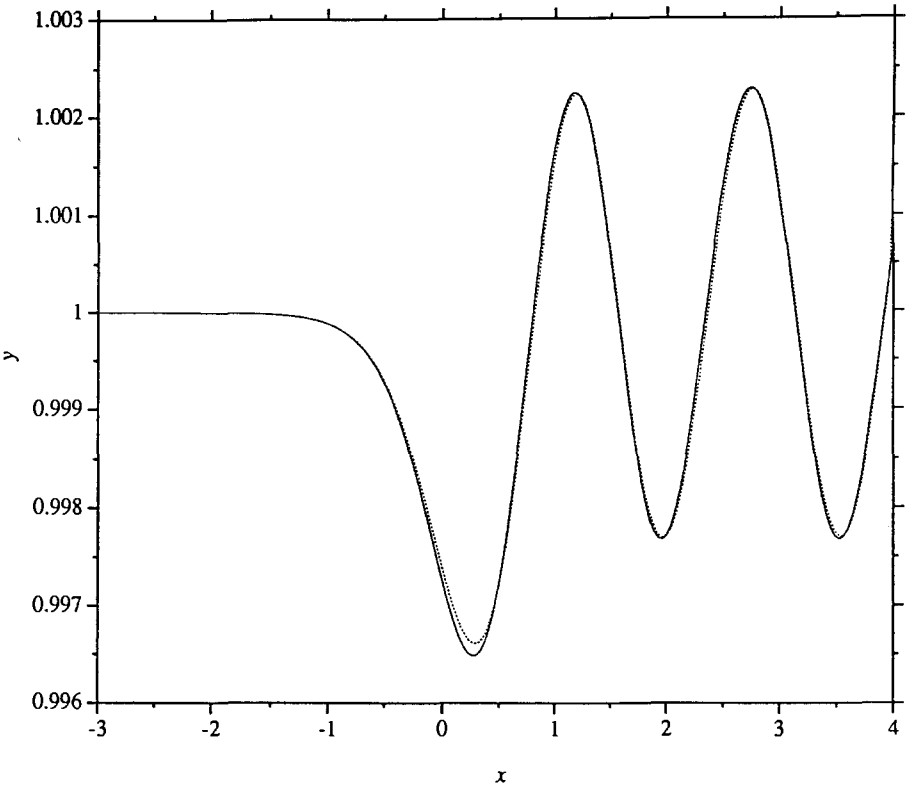

Fig. 3. Comparison of free-surface profiles calculated from the linearized model (solid line) and current nonlinear model (dotted line) for $\alpha = 0.05$ and $F = 0.5$.

the reference value for x, i.e., $x(\phi_{N+1}^{(1)})$. To avoid integrating (11) through the singularity at $\zeta = 0$, we assumed that $x(\phi_{N+1}^{(1)})$ is equal to the x value at $\phi = \phi_{N+1}^{(1)}$ on the bottom, which can be readily found by integrating (11) along the horizontal part of the bottom, because the flow is essentially uniform upstream. This technique was also used by Tuck and Goh [14].

4. Numerical results and discussion

As a first check, the nonlinear free-surface profile was compared with the linearized one for a small value of α. Good agreement between the two can be observed in Figure 3, which simply indicates that the linearized solution, or the first-order solution in a perturbation expansion, is a good approximation when α is small.

Next, we examined the rate of convergence of the numerical method. It is evident from Figure 4 that a converged solution is quickly attained under grid refinement. A quantitative examination can be conducted by defining the L_2-norm between two free-surface profiles as

$$L_{ij} = \left\{ \int_{x_1}^{x_2} [y_i(x) - y_j(x)]^2 \, \mathrm{d}x \right\}^{1/2}, \tag{24}$$

where x_1 and x_2 are the truncation points, and tabulating the results in Table 1, from which we can clearly see the sequence of norms indeed quickly diminishing as the grid is refined.

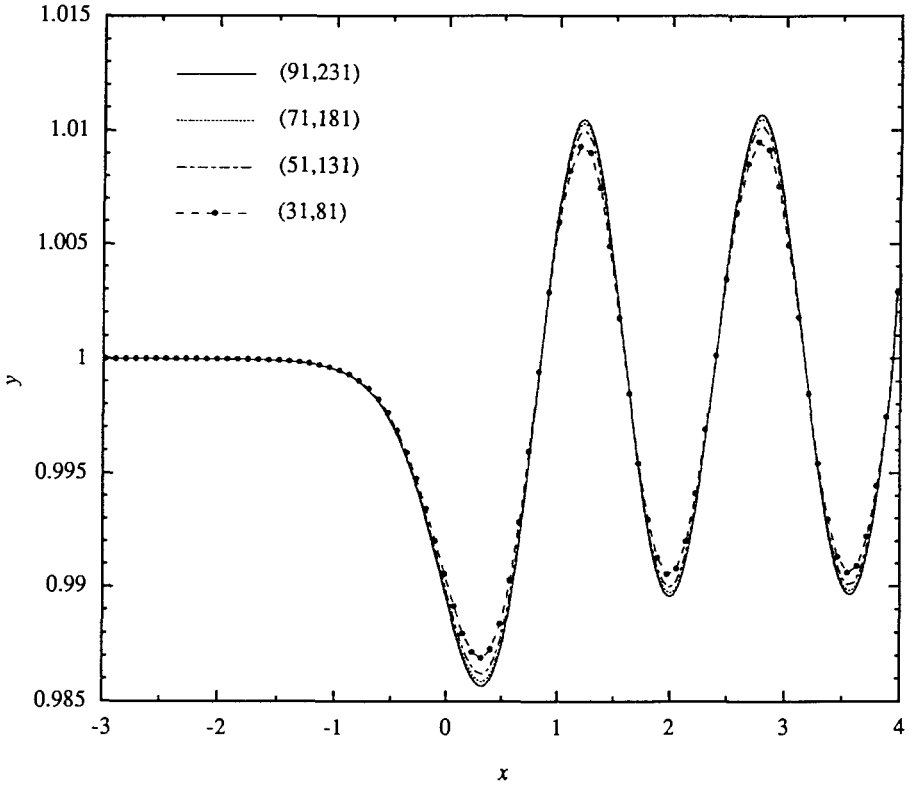

Fig. 4. Convergence of the nonlinear solution for the free-surface profile under grid refinement ($\alpha = 0.1, F = 0.5$). The pair of numbers in the parentheses refer to the number of nodes placed on the obstruction and the free surface respectively.

Table 1. L_2-norms between two adjacent free surfaces under grid refinement.

Number of nodes	(31, 81)* and (41, 106)	(41, 106) and (51, 131)	(51, 131) and (61, 156)
L_{ij}	3.83×10^{-3}	2.44×10^{-3}	1.70×10^{-3}
Number of nodes	(61, 156)* and (71, 181)	(71, 181) and (81, 206)	(81, 206) and (91, 231)
L_{ij}	1.25×10^{-3}	9.65×10^{-4}	7.67×10^{-4}

* The pairs of numbers refer to the number of nodes placed on the obstruction and the free surface, respectively.

With α being increased, the nonlinearity becomes more and more significant. As shown in Figure 5, when $\alpha = 0.2$, the peak-to-trough amplitude predicted from the nonlinear models is 88% larger than that from the linear model. Also shown in the same figure is Forbes and Schwartz's nonlinear solution. There is a reasonable agreement between the two nonlinear free-surface profiles almost everywhere, except upstream. By the adoption of the radiation condition (23), our model has successfully eliminated upstream 'spurious' waves which were present in Forbes and Schwartz's model, in which an integro-differential equation has to be solved. The spurious waves may be due to the presence of the derivatives of the unknowns in their model, which might have induced numerical instability under small numerical disturbances.

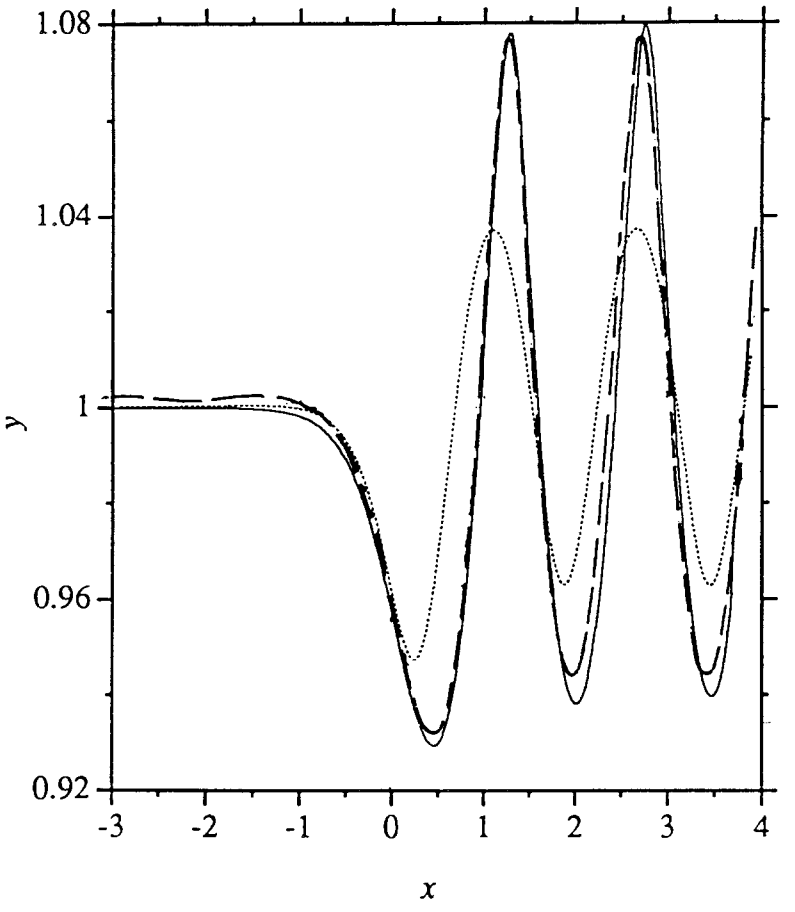

Fig. 5. Comparison of free-surface profiles calculated from the linearized model (dotted line), from Forbes and Schwartz's nonlinear model (dashed line), and from current nonlinear model (solid line) or $\alpha = 0.2$ and $F = 0.5$.

One of the most important features of a wave-like solution is the occurrence of a wave resistance or drag force acting on the obstruction, even in the absence of viscosity, due to the transportation of energy by the waves towards downstream. Here we define a drag coefficient D to be the horizontal component of the drag force, made dimensionless by reference to $\rho g h_0^2$.

Figure 6 shows the drag coefficients as a function of the disturbance α. It can be seen that for $\alpha < 0.15$, our results are a little smaller than those of Forbes and Schwartz [1], while for $\alpha > 0.15$, our results are a little larger. But in general the two nonlinear drag coefficients agree with each other reasonably well. From Figure 6 it is also evident that the nonlinearity is important for $\alpha > 0.13$.

Because for a semi-circular obstruction there exists a two-parameter family of solutions, one must also examine the variation of the drag coefficient as a function of the Froude number F. From Figure 7 one can see that for a small disturbance $\alpha = 0.1$, our results agree with the linearized ones for $F \geqslant 0.5$. In other words, the validity of the linearized model (in which α is treated as a small parameter) for small α seems to be hardly affected by the value of F. On the other hand, Forbes and Schwartz's results are significantly different from ours when $F \geqslant 0.7$. As $F \to 1$, the linearized model fails to yield a finite wave amplitude (due to resonance), but

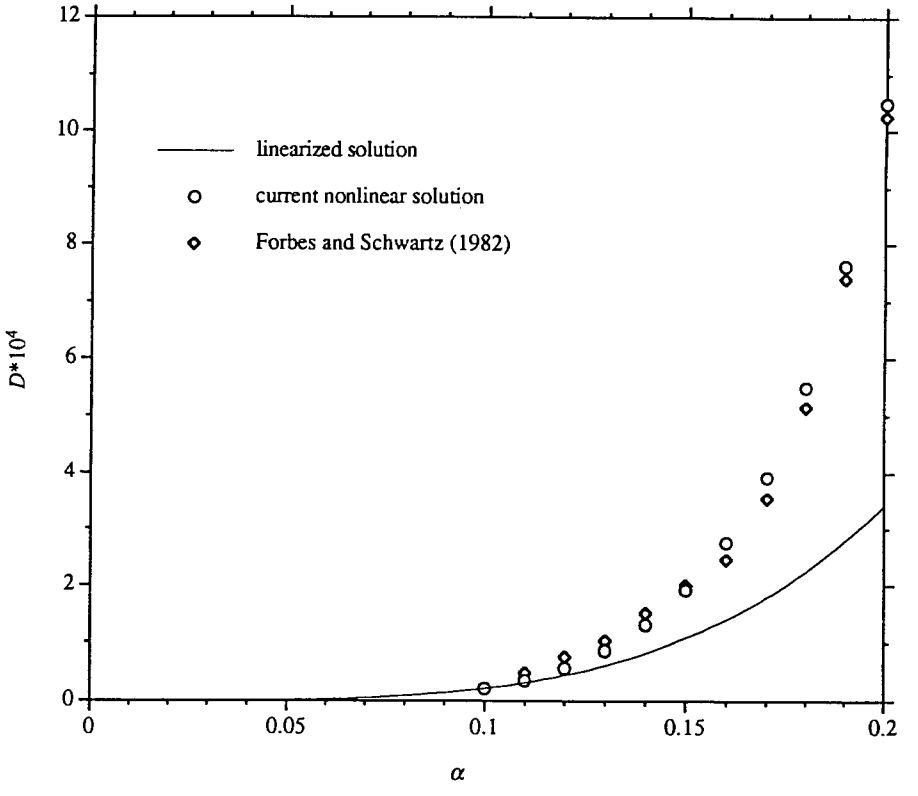

Fig. 6. Wave drag as a function of α for $F = 0.5$.

still gives a finite wave drag. This interesting phenomenon can be explained by looking at the linearized solution near $F = 1$. As $F \to 1$, the amplitude from the linear model approaches infinity and at the same time, the wavelength approaches infinity as well. On the other hand, the momentum flux, or the drag coefficient, approaches a limiting value of $\frac{3}{2}\pi^2\alpha^4$. However, the linear drag in the transcritical range (with F being close to 1), based on the assumption that a steady state can be eventually reached, is not realistic any more, since recent research [16,17] has revealed that in this range there exist no steady-state solutions. On the other hand, the corresponding nonlinear results from our numerical model, which assumes that a steady state can be eventually reached, are believed to be unrealistic as well. Numerically, as $F \to 1$, the wavelength becomes longer and longer, and thus more and more grid points are needed on the free surface, if a computational domain of a certain number of wavelengths needs to be maintained. Hence it becomes harder and harder to obtain a nonlinear solution as $F \to 1$. For example, when $\alpha = 0.1$ and $F \geqslant 0.9$, we can only compute one wavelength downstream with the computer resources available to us. It is believed that convergent solutions for $F \geqslant 0.9$ with two or even more wavelengths can be obtained if the current model is implemented on a computer with larger memory and faster speed. However, it should be remembered that even if a nonlinear solution is attained in the transcritical range (for the specific definition of the transcritical range, see [17]), it becomes non-physical according to [16,17], as it may never occur in reality. The bounds of the transcritical range in terms of the Froude number supplied by, say, [17], therefore serve as a good guide on whether the current steady-state model should be used.

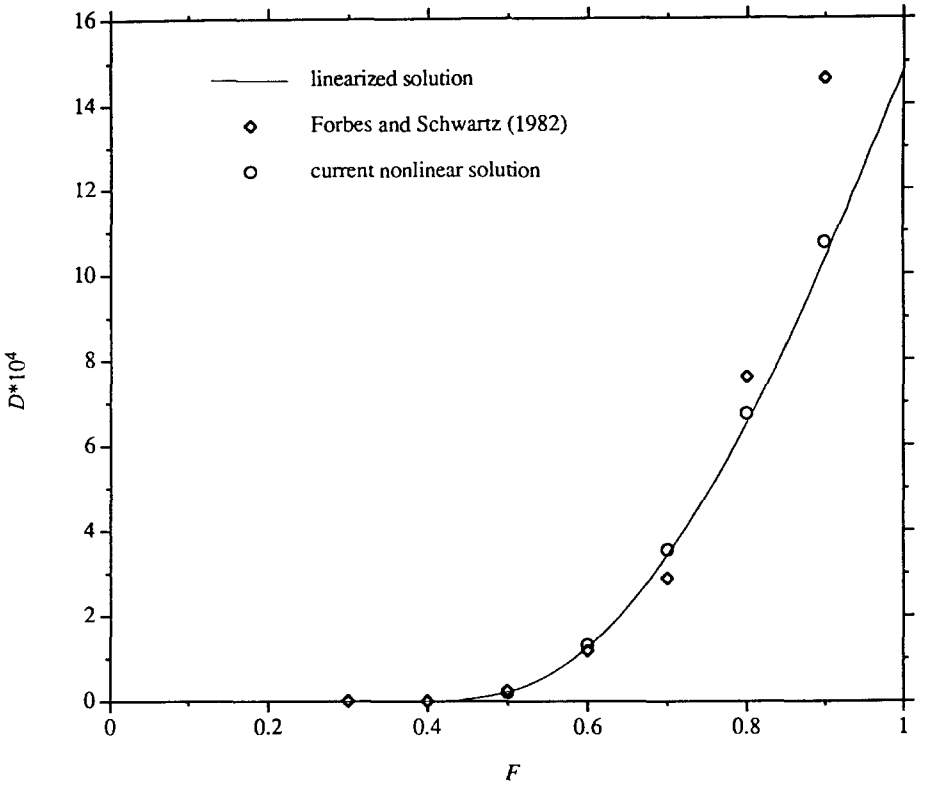

Fig. 7. Wave drag as a function of Froude number for $\alpha = 0.1$.

When F is decreased from $F = 0.5$, the linearized results start to lose accuracy, as shown in Figure 8, although the difference between the linear and nonlinear drag coefficients is only of order 10^{-6}. For $F < 0.4$, the drag is of order 10^{-8} or less, and it becomes extremely difficult to achieve a desired convergence with the computational facilities available to us; both the memory and speed required to carry out a satisfactory calculation increase dramatically. Nevertheless, the data shown in Figure 8 have already clearly indicated the breakdown of the linear solution. This somewhat bizarre phenomenon was previously referred to by Doctors and Dagan [12] and Dagan [5] etc. as 'small-Froude-number non-uniformity' (or 'second Froude number paradox'). Doctors and Dagan showed that, in an analogous problem of flow past a pressure distribution, as F was decreased the conventional perturbation theory began to break down because the higher-order terms suppressed the first-order term and nonlinearity was important in the range of small Froude numbers. Previous studies on this non-uniformity in Froude number were limited to the case of an infinite fluid depth; with our results at hand it is evident that the non-uniformity is also present for a finite fluid depth.

5. Conclusion

In this paper, a new integral-equation model based on hodograph variables is proposed to solve free-surface flow past an arbitrary obstruction with waves generated downstream. The numerical scheme suggested by Niessner [11] is adopted to solve the nonlinear integral equations.

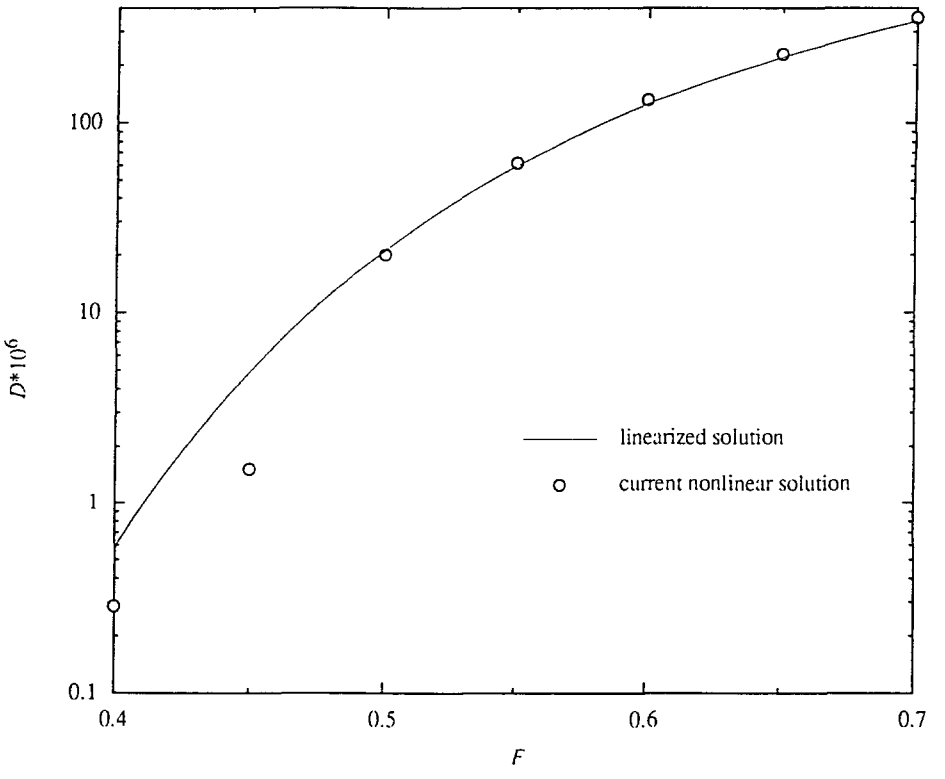

Fig. 8. Wave drag for small Froude numbers ($\alpha = 0.1$).

Numerical results for the case of a semi-circular obstruction are compared with those of Forbes and Schwartz [1]. In general, good agreements are observed between the two models. For a small obstruction, our results indicate that the linear model can be adopted to calculate the drag force for moderate and large Froude numbers up to the transcritical range, but fails for small Froude numbers due to the small-Froude-number non-uniformity.

Compared with previous models, the new model is more versatile and does not suffer from the upstream spurious waves. A further application of this model to other types of bottom irregularities has just been completed by the authors and the results have been reported elsewhere [15].

Acknowledgment

The first author would like to gratefully acknowledge the financial support from the DEET (Australia) providing the Overseas Postgraduate Research Scholarship (OPRS) and that from the University of Wollongong providing the University of Wollongong Postgraduate Research Award (UPRA) in carrying out this research project.

References

1. L.K. Forbes and L.W. Schwartz, Free-surface flow over a semicircular obstruction, *J. Fluid Mech.* 114 (1982) 299–314.
2. H. Lamb, *Hydrodynamics*, 6th edn. New York: Dover Publications (1945), 738 pp.

3. J.V. Wehausen and E.V. Laitone, Surface Waves, In: *Handbuch der Physik*, Vol. 9, S. Flugge (ed.), Berlin: Springer-Verlag (1960).
4. E.O. Tuck, The effect of non-linearity at the free-surface on flow past a submerged cylinder, *J. Fluid Mech.* 22 (1965) 401–414.
5. G. Dagan, Waves and wave resistance of thin bodies moving at low speed: the free-surface nonlinear effect, *J. Fluid Mech.* 69(2) (1975) 405–416.
6. F. Dias and J.-M. Vanden-Broeck, Open channel flows with submerged obstructions, *J. Fluid Mech.* 209 (1989) 155–170.
7. L.K. Forbes, Critical free-surface flow over a semi-circular obstruction, *J. Eng. Math.* 22 (1988) 3–13.
8. J.-M. Vanden-Broeck, Numerical solutions for cavitating flow of a fluid with surface tension past a curved obstacle, *Phys. Fluids* 27(11) (1984) 2601–2603.
9. J.-M. Vanden-Broeck and J.B. Keller, Pouring flows, *Phys. Fluids* 29(12) (1986) 3958–3961.
10. J.-M. Vanden-Broeck, Free-surface flow over an obstruction in a channel, *Phys. Fluids* 30(8) (1987) 2315–2317.
11. H. Niessner, Significance of kernel singularities for the numerical solution of Fredholm integral equations, *Boundar Elements* Vol. IX, C.A. Brebbia, W.L. Wendland, and G. Kuhn (eds.), Computational Mechanics, Southampton (1987).
12. L.J. Doctors and G. Dagan, Comparison of nonlinear wave-resistance theories for a two-dimensional pressure distribution, *J. Fluid Mech.* 98(3) (1980) 647–672.
13. D. Scullen and E.O. Tuck, Nonlinear free-surface flow computations for submerged cylinders, *J. Ship Res.* (in press).
14. E.O. Tuck and K.H.M. Goh, Thick waterfalls from horizontal slots, *J. Eng. Math.* 19 (1985) 341–349.
15. Y.-L. Zhang and S.-P. Zhu, A comparison study of nonlinear waves generated behind a semi-circular trench, *Proc. Roy. Soc. London Ser. A* (submitted).
16. T.R. Akylas, On the excitation of long nonlinear water waves by a moving pressure distribution, *J. Fluid Mech.* 141 (1984) 455–466.
17. T.Y. Wu, Generation of upstream advancing solitons by moving disturbances, *J. Fluid Mech.* 184 (1987) 75–99.
18. A.C. King and M.I.G. Bloor, Free-surface flow of a stream obstructed by an arbitrary bed topography, *Q. J. Mech. Appl. Math.*, 43(1) (1990) 87–106.